STRUCTURAL, MECHANICAL AND OPTICAL PROPERTIES OF ZINC-STRONTIUM-LITHIUM PHOSPHATE GLASS DOPED WITH CHITOSAN

Siti Norfariza Farhana Binti Mohd Razak
Advanced Optical Materials Research Group, Faculty of Science, Universiti Teknologi Malaysia

Adibah Hanisah Binti Samsudin
Advanced Optical Materials Research Group, Faculty of Science, Universiti Teknologi Malaysia

Nurhafizah Binti Hasim
Advanced Optical Materials Research Group, Faculty of Science, Universiti Teknologi Malaysia

Nur Hidayah Binti Ahmad
Advanced Optical Materials Research Group, Faculty of Science, Universiti Teknologi Malaysia

他

https://doi.org/10.5109/7395639

出版情報：Proceedings of International Exchange and Innovation Conference on Engineering & Sciences (IEICES). 11, pp.1029-1035, 2025-10-30. International Exchange and Innovation Conference on Engineering & Sciences
バージョン：

STRUCTURAL, MECHANICAL AND OPTICAL PROPERTIES OF ZINC-STRONTIUM-LITHIUM PHOSPHATE GLASS DOPED WITH CHITOSAN

Siti Norfariza Farhana Binti Mohd Razak[1], Adibah Hanisah Binti Samsudin[1], Nurhafizah Binti Hasim[1], Nur Hidayah Binti Ahmad[1], Norshahirah Binti Mohamad Saidi[1], Mohd Fuad Bin Mohamad[2],
[1] Advanced Optical Materials Research Group, Faculty of Science, Universiti Teknologi Malaysia, Johor, Skudai, 81310, Malaysia, [2] Department of Chemistry, Faculty of Science, Universiti Teknologi Malaysia, Johor, Skudai, 81310, Malaysia,
Corresponding email: nurhafizah.h@utm.my

Abstract: *Phosphate-based glasses offer advantages such as low melting temperatures and compositional flexibility but are limited by poor mechanical strength, optical performance, and low structural stability. The study investigates the effect of chitosan incorporation on the structural, mechanical, and physical properties of zinc-strontium-lithium phosphate glass. A series of glass samples with the composition (40 – x) P_2O_5 – 30 ZnO – 25 Li_2O – 5 SrO – (x) CS, where 0.0 ≤ x ≤ 1.0 mol%, was prepared using the melt-quenching technique. The samples were characterized using FTIR, Raman spectroscopy, ultrasonic testing and UV-Vis spectroscopy. FTIR and Raman analyses revealed structural changes in the glass network with increasing chitosan, while ultrasonic testing showed enhanced hardness and elastic moduli. UV-Vis spectroscopy demonstrated greater glass opacity with a higher chitosan content. These findings suggest chitosan doping is effective for tailoring multifunctional phosphate glass properties, with strong potential in biomedical and UV-blocking applications.*

Keywords: Phosphate Glass; Chitosan; FTIR; Ultrasonic Testing; UV-Vis.

1. INTRODUCTION

Phosphate glass can adjust to many changes for specialized properties due to its various network structures, high transparency, and density [1]. The low melting temperatures, high thermal expansion coefficient, and optical qualities [2] that are applicable to a wide range of technical applications are distinctive characteristics of phosphate glass that set it apart from other glasses. Phosphate glass tends to have poor chemical durability and low thermal and mechanical stability, so modifiers like ZnO, Li_2O, and SrO are added to strengthen the glass network, improve stability, and enhance its overall performance [3].

Zinc oxide (ZnO), strontium oxide (SrO), and lithium oxide (Li_2O) are examples of oxide elements that can be added as glass modifiers to produce high-quality glass. In phosphate glass, zinc oxide can increase the glass's chemical stability, stop hydration processes, and make it nearly insoluble in alcohol and water [4]. With a processing temperature below 400 ˚C, it was found that the zinc phosphate glasses were chemically resistant [5]. Strontium oxide (SrO) has also been shown in some earlier research to enhance the mechanical strength, chemical durability, and glass-forming properties of phosphate glass. Additionally, adding lithium carbonate (Li_2CO_3) or strontium carbonate ($SrCO_3$) to the phosphate glass matrix lowers phonon energy, which boosts luminescence efficiency and prolongs lifespan [6]. Adding lithium to phosphate glasses results in low melting temperatures, strong glass-forming properties [22], low glass transition temperatures, and high electro positivity, all of which improve glass conductivity [7].

Additionally, chitosan (CS) is an eco-friendly polymer derived from chitin, characterized by the presence of amino and hydroxyl groups. It is known for being biodegradable, biocompatible, antimicrobial, highly selective, and non-toxic [8]. Recent research has shown that is also possible for chitosan can be combined with other kind of substances, such as metal oxides [9]. Chitosan coatings have been demonstrated in recent research to greatly improve the durability and bioactivity of bioactive glasses [10].

While phosphate glasses have been extensively studied for their compositional flexibility and functional applications, the specific influence of chitosan incorporation on their structural, mechanical, and physical properties remains insufficiently explored. Limited studies have addressed how chitosan interacts with the phosphate glass network and its potential to enhance glass performance, indicating a need for deeper investigation in this area.

This study investigates the influence of chitosan doping on phosphate glasses with the concentrations of chitosan (0.0 - 1.0 mol%), with a focus on enhancing its overall performance.

2. METHOD & RESULT AND DISCUSSION

In these sub section, the method as well as the result and discussion of the sample will be presented and discussed.

2.1 Materials and Methods

Glass samples with the composition (40–*x*) P_2O_5 - 30 ZnO – 25 Li_2O – 5 SrO - (*x*) CS , where x ranges from 0 to 1 mol%, were prepared using the melt-quenching technique. A total batch mass of 15 g was used, with raw materials including phosphorus pentoxide (P_2O_5), lithium oxide (Li_2O), zinc oxide (ZnO), strontium carbonate ($SrCO_3$), and chitosan (CS), accurately weighed using an electronic balance.

The samples were labeled S1 through S6, as listed in Table 1. All components except P_2O_5 were first placed into a plastic bottle and homogenized using a milling machine for 30 minutes. Afterward, P_2O_5 was added, and the complete mixture was transferred to an alumina

crucible for preheating at 300 °C for 1 hour to eliminate moisture. The preheated mixture was then melted at 1000 °C for 30 minutes. The molten glass was poured onto a preheated metal plate and annealed at 300 °C for 3 hours to relieve internal stress.

A series of glass based of composition of (40-*x*) P_2O_5 - 30 ZnO - 25 Li_2O - 5 SrO - (*x*) CS where ($0.0 \leq x \leq 1.0$ mol%) for 15 g have successfully been prepared by using conventional melt-quenching technique. This procedure was repeated for all glass samples with varied mol% concentrations, as summarized in Table 1.

Table 1. The composition of (40-*x*) P_2O_5 - 30 ZnO - 25 Li_2O - 5 SrO - (*x*) CS where ($0 \leq x \leq 1$ mol%)

Sample	Composition (mol%)				
	P_2O_5	ZnO	Li_2O	SrO	CS
S1	40.0	30.0	25.0	5.0	0.0
S2	39.8	30.0	25.0	5.0	0.2
S3	39.6	30.0	25.0	5.0	0.4
S4	39.4	30.0	25.0	5.0	0.6
S5	39.2	30.0	25.0	5.0	0.8
S6	38.0	30.0	25.0	5.0	1.0

Fourier Transform Infrared (FTIR) spectroscopy was employed to analyze the transmission and absorption characteristics of the bulk glass samples. The measurements were carried out using a PerkinElmer Spectrum GX FT-Infrared Spectrometer. All spectra were obtained using the Attenuated Total Reflectance (ATR) mode, covering a spectral range of 4000–650 cm^{-1} with a resolution of 4 cm^{-1}. The FTIR data were background corrected and subsequently analyzed using the PerkinElmer Frontier GP0B FTIR Spectrometer.

Raman spectroscopy was utilized to investigate structural changes surrounding the phosphate atoms in the glass samples. As a technique complementary to infrared (IR) spectroscopy, Raman provides vibrational information that is often inaccessible through IR alone. Measurements were conducted using a Micro Raman Mapping System, Model: Unidron – A (2019), operating within a spectral range of 4000–100 cm^{-1} and an acquisition time of 10 seconds. The bulk samples were excited using an argon ion laser with a power output of 20 mW. For accurate spectral analysis, each sample was carefully positioned on the sample holder, and the microscope stage and control knobs were adjusted to ensure precise alignment under the optical lens.

Ultrasonic measurement was conducted to evaluate the material properties, dimensions, and flaw detection of the glass samples at room temperature using the pulse-echo technique. The analysis was carried out with an Ultrasonic Data Acquisition System (Matec 8020, Matec Instruments, USA) operating at a resonant frequency of 5 MHz. The system comprises three main components: a pulser-receiver, a transducer, and an oscilloscope, supported by a power supply unit providing the necessary direct current to the devices.

Key parameters such as time of flight, amplitude, and frequency were extracted from the waveform analysis. Prior to scanning, a coupling medium (essential oil) was applied between the glass surface and the ultrasonic probe to eliminate air gaps, ensuring efficient transmission of ultrasonic waves. Pulses generated by the pulse oscillator were converted into acoustic signals by the transmitting transducer, transmitted through the sample, and then reconverted into electrical signals by the receiving transducer. These signals were visualized on the oscilloscope for analysis. The information displayed was taken to calculate the elastic constant measurements, which can be evaluated by using Equation (1) to (8).

$$\text{Longitudinal Velocity: } V_L = \frac{2d}{\Delta T} \quad (1)$$

$$\text{Shear Velocity: } V_S = \frac{2l}{(\Delta T)} \quad (2)$$

$$\text{Longitudinal Modulus: } L = \rho V_L^2 \quad (3)$$

$$\text{Shear Modulus: } G = \rho V_S^2 \quad (4)$$

$$\text{Bulk Modulus: } K = L - \frac{4}{3}G \quad (5)$$

$$\text{Young's Modulus: } E = 2G\,(1 + \sigma) \quad (6)$$

$$\text{Poisson's ratio: } \sigma = \frac{(1-2G)}{2(L-G)} \quad (7)$$

$$\text{Microhardness: } H = \frac{(1-2\sigma)E}{[6(1+\sigma)]} \quad (8)$$

For UV-Vis characterization, each bulk glass sample was directly placed into the Shimadzu UV-3101PC scanning UV-Vis spectrophotometer (Kyoto, Japan) for analysis, using air as the reference. Spectral data were collected over the wavelength range of 200 to 1600 nm, and the results were expressed in terms of percent transmittance. Specific values for transmittance at 600 nm and absorbance at 500 nm were recorded for further analysis. Equation 9 shows how the transparency of the films was determined.

$$\%\text{Transparency} = \frac{2-T_{600}}{t} \quad (9)$$

2.2 Results and Discussion

The corresponding phosphate glass were measured by the Fourier Transform Infrared Spectroscopy (FTIR) spectroscopy in Attenuated-Total Reflection (ATR) mode. The ATR-FTIR spectra of (40 - *x*) P_2O_5 - 30 ZnO - 25 Li_2O - 5 SrO – (*x*) CS where ($0.0 \leq x \leq 1.0$ mol%) glass system that consist of six absorption bands are shown (see Fig.1). Each band relates to the vibration of a particular functional group. The absorption peaks positions were summarized in Table 2 shows the suggested assignment which introduced to interpret the observed infrared bands.

Table 2. The FTIR peaks positions of (40 - *x*) P_2O_5 - 30 ZnO - 25 Li_2O - 5 SrO (*x*) CS where ($0.0 \leq x \leq 1.0$ mol%)

Sample	IR Band (cm^{-1})					
1	740	886	1083	1222	1602	3442
2	737	877	1076	1236	1600	3420
3	733	890	1079	1264	1600	3480
4	730	881	1081	1241	1602	3480
5	740	890	1078	1234	1601	3425
6	733	881	1076	1244	1605	3387

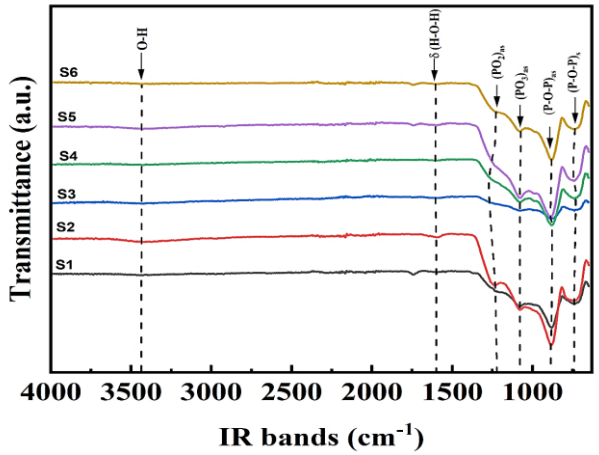

Fig. 1. FTIR spectra of (40 - x) P_2O_5 - 30 ZnO - 25 Li_2O - 5 SrO (x) CS where ($0.0 \leq x \leq 1.0$ mol%).

Table 3. The band position of FTIR spectra of (40–x) P_2O_5 - 30 ZnO - 25 Li_2O - 5 SrO - (x) CS where ($0 \leq x \leq 1$ mol%)

No.	IR Band ($\pm$0.1 cm^{-1})	Assignments
1	730-740	Symmetric stretching vibration of P-O-P bridges, vs (P-O-P)
2	877-890	Asymmetric stretching vibration of P-O-P bridges, vs (P-O-P)
3	1076-1083	vs (P-O-P) of PO_3 asymmetric stretching band
4	1222-1264	vs (P-O-P) of PO_2 asymmetric stretching band
5	1600-1605	H-O-H bending vibration
6	3387-3480	Fundamental stretching of O-H groups

Table 3 shows the band position of FTIR spectra of the glass system. The band observed between 730–740 cm^{-1} is linked to the symmetric stretching of the bridging oxygen in the P–O–P group, which indicates the breakdown (depolymerization) of the phosphate network and shortening of its chains [1,11]. The bands between 877–890 cm^{-1} are associated with the asymmetric stretching of P–O–P linkages and are known to vary with different metaphosphate ring structures [12]. The absorption band around 1076 cm^{-1} corresponds to the asymmetric stretching of PO_3 groups, which are characteristic of Q^1 units, typically found at the ends of phosphate chains [11]. A band near 1222 cm^{-1} is related to the asymmetric stretching of non-bridging oxygen in Q^2 phosphate tetrahedra [13]. The broad band between 1600 and 4000 cm^{-1} is due to O–H bending vibrations from water molecules [14]. Additionally, the band between 3387 and 3480 cm^{-1} is attributed to O–H stretching vibrations, indicating the moisture-absorbing nature (hygroscopicity) of phosphate glass [11].

Raman spectroscopy is used to identify different structural units and observe changes in these units caused by the addition of modifier ions. Its results complement those from FTIR analysis. Raman scattering involves lower inelastic energy compared to vibrational energy, with wave numbers typically ranging from 100 to 1500 cm^{-1}. Fig. 2 and Fig. 3 show the Raman spectra of the prepared glass samples and the deconvoluted spectra for S1, respectively. The Raman shift values are listed in Table 4, and the six main spectral regions are summarized in Table 5.

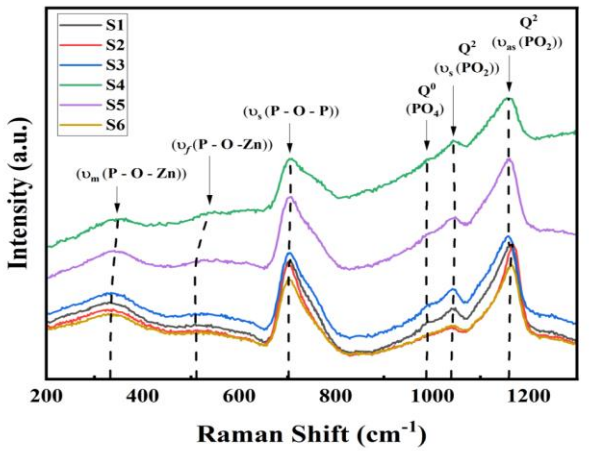

Fig.2. Raman shifts spectra of (40-x) P_2O_5 - 30 ZnO – 25 Li_2O - 5 SrO - (x) CS where ($0.0 \leq x \leq 1.0$ mol%) glass system.

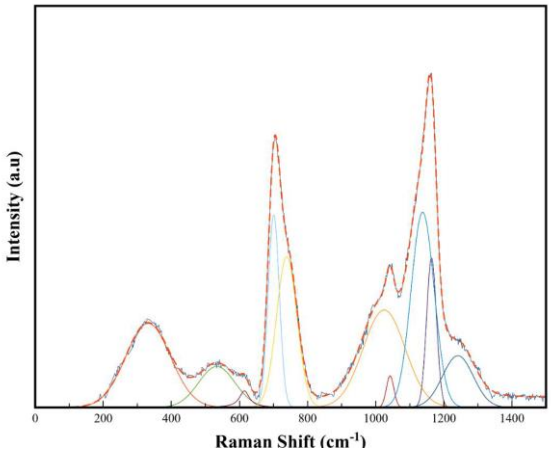

Fig.3. Deconvolution of Raman spectra of (40-x) P_2O_5 - 30 ZnO – 25 Li_2O - 5 SrO - (x) CS where x is 0.0 mol% glass system.

Table 4. Raman shifts position of (40-x) P_2O_5 - 30 ZnO - 25 Li_2O−5 SrO−(x) CS where ($0.0 \leq x \leq 1.0$ mol%) glass system

Sample	Raman Shifts (cm^{-1})					
	δm (P-O-Zn)	δf (P-O-Zn)	υs (P–O–P)	Q^0 PO_4	Q^2 υs (PO_2)	Q^2 (υas (PO_2))
1	334	542	705	989	1043	1159
2	334	541	703	990	1041	1168
3	334	541	703	988	1043	1157
4	346	549	705	989	1044	1157
5	344	550	705	988	1047	1158
6	333	540	703	990	1041	1164

Fig. 2. shows the Raman spectrum of phosphate glass, with the strongest band appearing at 1157–1168 cm^{-1} and a weaker band at 331–344 cm^{-1}. These vibrations come from the phosphate network and may also be influenced by the presence of zinc oxide. The 331–344 cm^{-1} band is linked to torsional vibrations (bending) involving P–O–Zn bonds, indicating zinc is acting as a modifier [17]. A sharp peak between 540 and 550 cm^{-1} also relates to

bending vibrations in the zinc-phosphate structure. The band at 703–705 cm^{-1} is due to asymmetric stretching of P–O–P bonds in metaphosphate chains [15]. The band around 988–990 cm^{-1} corresponds to symmetric stretching of P–O bonds in PO_4 units. Vibrations in the 1041–1047 cm^{-1} range are from symmetric stretching of non-bridging oxygens (PO_2 groups, Q^2 units).

Table 5. Raman shifts of (40-x) P_2O_5 - 30 ZnO - 25 Li_2O - 5 SrO - (x) CS where ($0.0 \leq x \leq 1.0$ mol%) glass system

No.	Raman Shift (cm^{-1})	Assignments
1	331-344	Bending vibration of P – O – Zn [15]
2	540-550	Bend mode related to zinc-phosphate network or ZnO4, (δm (P-O-Zn)) [16]
3	703-705	υs (P – O – P) of (BO) in Q2 mode [12]
4	988-990	Symmetric P – O stretching motions of PO_4 units
5	1041-1047	Symmetric stretching of $(PO_2)^-$ vibration (υs (PO_2), Q^2)
6	1157-1168	Asymmetric stretching of $(PO_2)^-$ vibration (υas (PO_2), Q^2)

The most intense band at 1157–1168 cm^{-1} is due to asymmetric stretching of non-bridging oxygen atoms bonded to phosphorus. The intensity of this band decreases with the addition of ZnO, suggesting that ZnO may reduce non-bridging P=O bonds and replace them with stronger Zn–O–P bridging bonds. These Zn–O–P bonds are more resistant to water than P–O–P or P–O–Zn^+ bonds [18]. At higher doping levels, chitosan (CS) does not cause the appearance of a distinct vibrational peak. This suggests that the CS is well-dispersed in the glass and does not form clusters. Since the CS content is less than 1% (0 to 1 mol%), it does not significantly affect the vibrations of the glass structure [19]. As the amount of CS increases, the Raman bands shift to higher wave numbers, which indicates the formation of more bridging oxygen bonds. Ultrasonic testing was performed on the samples to evaluate their elastic properties under low stress. This technique provided both the longitudinal and shear elastic constants of the glass samples. The main goal was to measure the longitudinal (L) and shear wave (G) velocities using the pulse-echo method and then use these values to calculate mechanical properties such as Young's modulus (E), bulk modulus (K), microhardness (H), and Poisson's ratio (σ) as shown in Table 6 and Table 7.

Table 6. The longitudinal and shear velocities with different CS composition

Mol% of CS	Longitudinal Velocity, V_L (ms^{-1})	Shear Velocity, V_s (ms^{-1})
1	4534	3287
2	4843	3802
3	5784	4804
4	5118	4201
5	4524	3280
6	3623	3078

Table 7. Variation of elastic moduli and Poisson's ratio with addition of CS

Mol % of CS	L (GPa)	G (GPa)	K (GPa)	E (GPa)	σ (GPa)
0.00	59.477	31.263	17.793	59.148	-0.054
0.20	70.108	43.196	12.513	60.255	-0.303
0.40	101.188	69.816	8.100	54.078	-0.613
0.60	78.771	53.084	7.992	49.550	-0.533
0.80	60.548	31.826	18.113	60.213	-0.054
1.00	36.628	26.444	1.369	10.667	-0.798

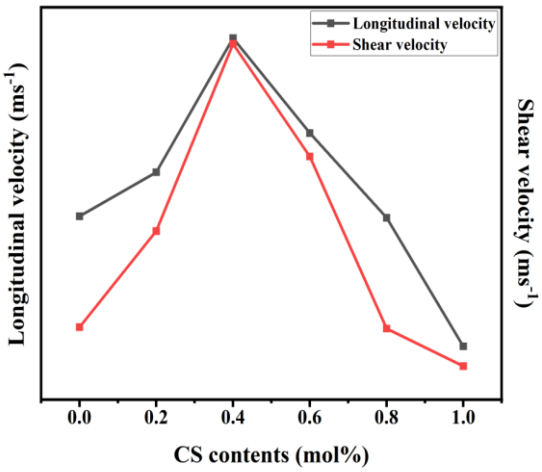

Fig. 4 (a). Ultrasonic longitudinal and shear wave velocities against CS concentration (mol%).

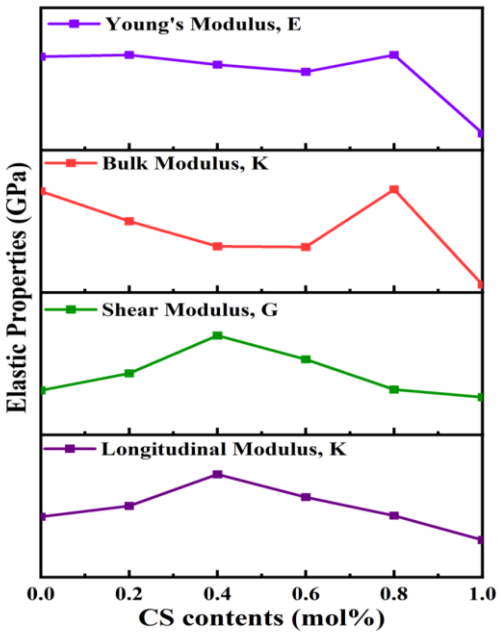

Fig. 4 (b). The variation of elastic moduli with different mol% of CS.

The ultrasonic velocities measured in the samples were found to be sensitive to changes in the glass composition, as shown in Table 6. The results show that as the chitosan

(CS) content increases, both longitudinal and shear wave velocities also increase up to a certain point. From Fig. 4 (a) and (b) and Table 7, it can be seen that the elastic moduli generally decrease with the addition of CS. The longitudinal modulus (L) increases from 59.477 to 101.188 GPa when CS content is up to 0.4 mol%, showing that the glass becomes more rigid and the network structure gets stronger [13]. However, with more CS (up to 1.0 mol%), L decreases again to 36.628 GPa. This nonlinear trend is also seen in the shear modulus. Young's modulus (E) decreases from 59.148 to 54.078 GPa with CS up to 0.6 mol%, then slightly increases at 0.8 mol%, and decreases again at 1.0 mol%. The bulk modulus (K) shows a similar pattern. The changes in longitudinal and shear velocities match the density values, which increase from 2.89 to 3.02 g/cm³ and then decrease to 2.79 g/cm³. Sample 3, with 0.6 mol% CS, has the highest density, indicating the greatest compactness and rigidity. This supports the trends seen in the velocity and elastic moduli data.

Table 8. Microhardness (H) and Poisson's ratio (σ) of glass structure with different CS contents

Mol% of CS	Poisson's Ratio, σ	Microhardness,H (GPa)
0.00	-0.054	11.547
0.20	-0.303	23.111
0.40	-0.613	51.790
0.60	-0.533	36.567
0.80	-0.054	11.755
1.00	-0.798	22.888

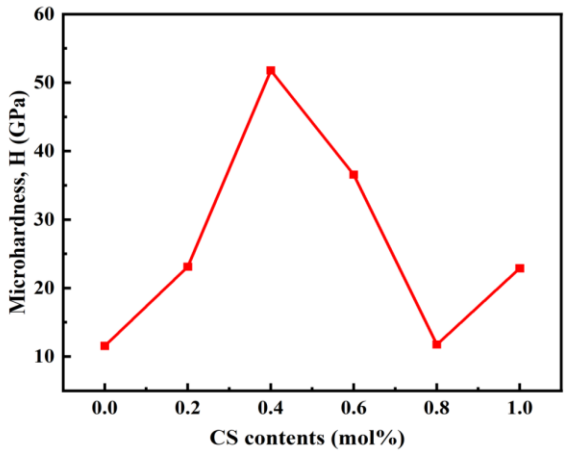

Fig. 5 (a). Microhardness, H and Poisson's ratio, σ of composition (40 – x) P_2O_5 – 30 ZnO – 25 Li_2O – 5 SrO – (x) CS where (0.0≤x≤1.0 mol%) glass system.

Poisson's ratio is useful for assessing the rigidity of glass samples with higher values indicate a more tightly packed glass network, and lower values suggest a looser structure. Fig. 5 (a) show the microhardness (H) against the Poisson's ratio (σ) graph. Table 7 and Table 8 show the measured Poisson's ratio (σ) and microhardness (H) values of the glass samples. As the CS content increases, the Poisson's ratio decreases, then increases, and decreases again. This trend is opposite to that of microhardness. The microhardness (H) increases from 11.547 to 51.790 GPa as CS content rises to 0.4 mol%, showing improved rigidity. However, H then drops from 36.567 to 22.888 GPa, indicating a reduction in glass rigidity [20]. At the same time, Poisson's ratio (σ) decreases from -0.054 to -0.613 as CS concentration increases. This behavior is likely due to increased ionicity in the glass network, caused by stronger polar bonds introduced by the modifiers [13]. The overall decreasing trend of Poisson's ratio, as shown in Fig. 5 (b), reflects a weakening of the glass network structure and a reduction in its rigidity.

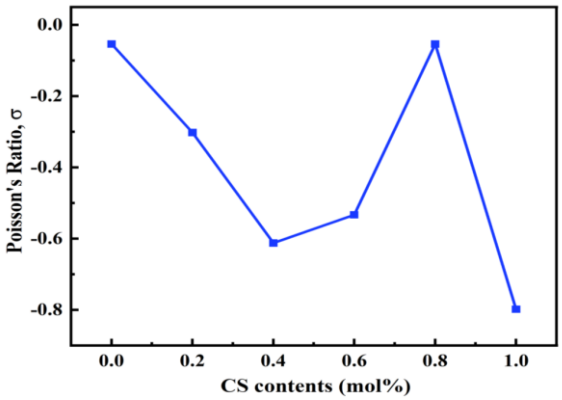

Fig. 5 (b). Poisson's ratio, σ of (40 – x) P_2O_5 – 30 ZnO – 25 Li_2O – 5 SrO – (x) CS where (0.0≤x≤1.0 mol%) glass system.

UV-Vis spectroscopy was used to analyze the optical properties of the (40 – x) P_2O_5 – 30 ZnO – 25 Li_2O – 5 SrO – (x) CS glass system, where 0.0 ≤ x ≤ 1.0 mol%. The spectra for each glass sample were recorded in the wavelength range of 200 to 800 nm to study their light transmission behavior. The results are expressed as percentage transmittance. Fig. 6 (a) and (b) show the UV-blocking effect in the spectra and the light absorbance properties of both the glass system and chitosan (CS), respectively.

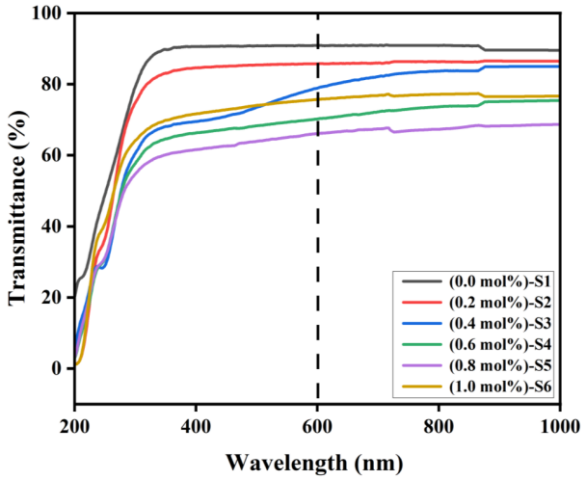

Fig. 6 (a). Light transmission properties of the glass system and chitosan.

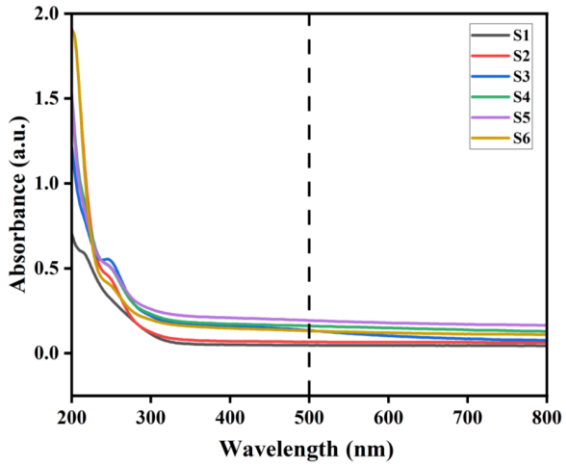

Fig. 6 (b). Light absorbance properties of the glass system and chitosan.

Fig. 6 (a) and (b) show the graph of light transmission and absorbance properties of the glass sample. The glass samples showed low light transmission in the UV region, especially around 280 nm. For the visible and near-infrared range (400–1000 nm), the pure glass sample without CS achieved up to 90% transmittance. The sample with 0.2 mol% CS showed around 85% transmittance in this range, while the 0.4 mol% CS sample reached nearly 85% between 880 and 1000 nm. At 875 to 1000 nm, the sample with 0.6 mol% CS had about 75% transmittance, and the 1.0 mol% CS sample reached nearly 76%. The 0.8 mol% CS sample showed the lowest transmittance, around 68%. Overall, the transmittance of the glass samples tends to decrease as the CS content increases. At 600 nm, the sample without CS showed the highest transmittance at 90%, while the 0.8 mol% CS sample had the lowest, nearly 65%.

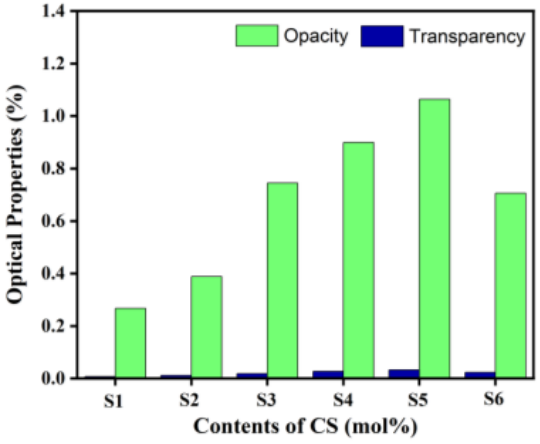

Fig. 7. Transparency values of (40 - x) P_2O_5 - 30 ZnO - 25 Li_2O - 5 SrO - (x) CS where ($0.0 \leq x \leq 1.0$ mol%) glass system.

Fig. 7 shows the transparency values of the glass samples. Sample S5, which contains 0.8 mol% CS, exhibited the highest opacity, with the lowest light transmission in the visible region. A noticeable change in the visible spectra is observed with the addition of chitosan. The increased opacity in S5 is likely due to the uniform dispersion of CS and changes in the internal structure of the glass, which reduces the amount of light passing through the material [21].

3. CONCLUSION

This study demonstrated that chitosan signifacantly influences the structural, mechanical and physical properties of zinc-strontium-lihium phosphate glass. Increasing chitosan concentration can led to a higher hardness, transparency and noticeable changes in the glass network. These finding suggest that chitosan-doped phosphate glass has strong potential for biomedical applications and UV-blocking materials. Future studies should explore higher chitosan concentrations and alternative dopants to further enhance glass performance.

4. ACKNOWLEDGEMENT

We would like to express our sincere gratitude for the financial support provided by the Fundamental Research Grant Scheme (FRGS) [R.J130000.7854.5F635 (PY/2023/02164)] and the Nippon Sheet Grant (International Grant) [R.J130000.7354.4B743 (PY/2021/02736)]. Additional support was received from the University Industry Research Lab (UIRL), PPMU, UTM under Dana Universiti Penyelidikan (Caj Analisis Makmal) [Q.J091600.3100.00A37].
We also gratefully acknowledge the support from the Team Experimental and Computational (TEC), Advanced Optical Materials Research Group (AOMRG), and the Assistant Science Officers from the Faculty of Science, UTM.

5. REFERENCES

[1] E.M. Bouabdalli, M. El Jouad, S. Touhtouh, et al., First investigation of the effect of strontium oxide on the structure of phosphate glasses using molecular dynamics simulations, Comput. Mater. Sci. 220 (2023) 112068.
[2] S. Toyoda, K. Sugamura, Y. Kuromitsu, K. Morinaga, Thermal expansion coefficient and working temperature of SrO–ZnO–P_2O_5 glasses, Rep. Fac. Eng. Kyushu Univ. 24 (2) (2002) 173–177. https://doi.org/10.15017/16660
[3] L. Han, Q. Zhang, J. Song, Z. Xiao, Y. Qiang, X. Ye, W. You, A. Lu, A novel Eu^{3+}-doped phosphate glass for reddish orange emission: Preparation, structure and fluorescence properties, J. Lumin. 221 (2020) 117041. https://doi.org/10.1016/j.jlumin.2020.117041
[4] A.A. Ogwu, A.M. Oje, J. Kavanagh, The properties of zinc sodium phosphate glass system with the various concentration of chromium oxide doped, J. Phys. Conf. Ser. 1280 (2019) 022079. https://doi.org/10.1088/1742-6596/1280/2/022079
[5] K.A. Matori, et al., Studying the effect of ZnO on physical and elastic properties of $(ZnO)x(P_2O_5)_{1-x}$ glasses using nondestructive ultrasonic method, Adv. Mater. Sci. Eng. 2015 (2015) 6 pages. https://doi.org/10.1155/2015/304802
[6] E.M. Bouabdalli, et al., Structural studies on varied concentrations of europium doped strontium phosphate glasses, Mater. Today: Proc. 66 (2022) 349–352. https://doi.org/10.1016/j.matpr.2022.05.450
[7] M.A. Ouis, et al., Thermal, mechanical and electrical properties of lithium phosphate glasses doped with copper oxide, Bull. Mater. Sci. 42 (2019) 5. https://doi.org/10.1007/s12034-019-1897-y

[8] H. Suryanto, U. Yanuhar, N.A.A. Fikri, G. Mahasri, Chlorella vulgaris-mediated nanosilver synthesis with chitosan capping agent, Evergreen 10 (1) (2023) 146–154. https://doi.org/10.5109/6781061
[9] Y. Bao, Q. Zhou, M. Zhang, H. Zhang, Q. Luan, W. Zhou, H. Tang, F. Huang, Wet-spun nanoTiO_2/chitosan nanocomposite fibers as efficient and retrievable absorbent for the removal of free fatty acids from edible oil, Carbohydr. Polym. 210 (2019) 119–126. https://doi.org/10.1016/j.carbpol.2019.01.035
[10] S. Spriano, G. Riccucci, G. Örlygsson, C. Ng, E. Vernè, F. Sehn, P. De Oliveira, S. Ferraris, Coating of bioactive glasses with chitosan: The effects of the glass composition and coating method on the surface properties, including preliminary in vitro results, Surf. Coat. Technol. 470 (2023) 129824. https://doi.org/10.1016/j.surfcoat.2023.129824
[11] N. Radouane, et al., Thermal, electrical and structural characterization of zinc phosphate glass matrix loaded with different volume fractions of the graphite particles, J. Non-Cryst. Solids 536 (2020) 119989. https://doi.org/10.1016/j.jnoncrysol.2020.119989
[12] S.A.M. Azmi, et al., Modification of structural and physical properties of samarium doped zinc phosphate glasses due to the inclusion of nickel oxide nanoparticles, J. Non-Cryst. Solids 411 (2015) 53–58. https://doi.org/10.1016/j.jnoncrysol.2014.12.024
[13] M.A. Algradee, et al., Evaluation of structural, elastic properties and nuclear radiation shielding competence of Nd^{3+} doped lithium-zinc-phosphate glasses, J. Non-Cryst. Solids 576 (2022) 121304. https://doi.org/10.1016/j.jnoncrysol.2021.121304
[14] B. Narsimha, K.C. Sekhar, R. Gokarakonda, Copper doped strontium indium-borate glasses: FTIR, Raman, EPR, optical and structural studies, Mater. Today: Proc. (2023) 2–9. https://doi.org/10.1016/j.matpr.2023.05.185
[15] N.N. Yusof, et al., Spectrographic analysis of zinc-sulfate-magnesium-phosphate glass containing neodymium ions: Impact of silver–gold nanoparticles plasmonic coupling, J. Lumin. 242 (2022) 118571. https://doi.org/10.1016/j.jlumin.2021.118571
[16] R.K. Brow, et al., The short-range structure of zinc polyphosphate glass, J. Non-Cryst. Solids 309 (1995) 3093–3098.
[17] A. Langar, et al., Structure and electrical characterization of ZnO–Ag phosphate glasses, Results Phys. 7 (2017) 1022–1029. https://doi.org/10.1016/j.rinp.2017.02.028
[18] M.A. Farag, et al., Enhancement of structural and optical properties of transparent sodium zinc phosphate glass–ceramics nanocomposite, J. Aust. Ceram. Soc. 58 (2) (2022) 653–661. https://doi.org/10.1007/s41779-022-00716-3
[19] D. Tuschel, Effect of dopants or impurities on the Raman spectrum of the host crystal, Spectroscopy 32 (12) (2017) 13–19.
[20] M.S. Gaafar, H.A. Afifi, M.M. Mekawy, Structural studies of some phospho-borate glasses using ultrasonic pulse-echo technique, DSC and IR spectroscopy, Physica B Condens. Matter 404 (12–13) (2009) 1668–1673. https://doi.org/10.1016/j.physb.2009.01.045
[21] B. Khanzada, B. Mirza, A. Ullah, Chitosan-based bio-nanocomposites packaging films with unique mechanical and barrier properties, Food Packag. Shelf Life 35 (2023) 101016. https://doi.org/10.1016/j.fpsl.2022.101016
[22] H. Masuda, Formation and structure of RO–Ga_2O_3 glasses (R = Ca, Sr, Ba), Rep. Fac. Eng. Sci. Kyushu Univ. 17 (2) (1995) 197–203. https://doi.org/10.15017/17372